McMaster University

Advanced Optimization Laboratory

Title:

Optimal Nearly-Analytic Discrete Approximation to the Scalar Wave Equation

Authors:

Dinghui Yang, Jiming Peng, Ming Lu and Tamás Terlaky

AdvOl-Report No. 2004/8

July 2004, Hamilton, Ontario, Canada

Optimal Nearly-Analytic Discrete Approximation to the Scalar Wave Equation

Dinghui Yang[1], Jiming Peng[2], Ming Lu[1], and Tamas Terlaky[2]
[1]Department of Mathematical Sciences, Tsinghua University, Beijing 100084, P. R. China
(dhyang@math.tsinghua.edu.cn)

[2]Department of Computing and Software, McMaster University, Hamilton, Canada
(pengj@mcmster.ca, terlaky@mcmaster.ca)

Submit the manuscript to *Geophysical Journal International* in July 2004

Abstract

Recently, we proposed the so-called optimal nearly-analytic discrete method (ONADM) for computing synthetic seismograms in acoustic and elastic wave problems (BSSA, Yang *et al.*, 2004). In this paper, we explore the theoretical properties of the ONADM including the stability criteria of the ONADM for solving one-dimensional (1-D) and two-dimensional (2-D) scalar wave equations, dispersion relations, and theoretical error. For comparison in the 1-D case, we also discuss numerical dispersions and stability criteria of the so-called Lax-Wendroff schemes with O(4,8), O(4,10), and the pseudo-spectral method (PSM). We then apply the ONADM to the heterogeneous case in synthetic seismograms. Promising numerical results illustrate that the ONADM provides a useful tool for large-scale heterogeneous practical problems as it can suppress effectively numerical dispersions caused by discretizing the wave equations when too-coarse grids are used.

Key Words: Optimal nearly-analytic discretization, scalar wave equation, heterogeneous media, synthetic seismogram, numerical dispersion, stability condition.

1 Introduction

Numerical methods for solving wave equations have provided useful tools in exploration seismology. In the forward modeling, the wave equation is typically used as an interpretive aid in complex geology or as a benchmark for testing processing algorithms. In waveform inversion for determining the earth structure, the accurate and efficient calculation of synthetic seismograms plays a key role. To solve the wave equation, we usually refer to two kinds of approximate methods. One approximate method is the perturbation method and the other is the discretization method in which we first discretize the wave equation and then solve the resulting finite-difference equations.

On the basis of finite-difference (FD) approximating directly the spatial and temporal derivatives in the wave equation, many numerical methods such as second-order center scheme (Kelly *et al.*, 1976), high-order compact schemes (or the so-called Lax-Wendroff (L-W) scheme (Dablain, 1986)), and the so-called optimally accurate schemes (Geller & Takeuchi, 1998) have been developed in the passed two decades. There are also other methods that use the PSM to compute spatial derivatives (e.g. Kosloff & Baysal, 1982). In our recent works (Yang *et al.*, 2002, 2004), we have briefly discussed various theoretical properties of these algorithms.

As a perturbation method, we recently proposed a so-called “optimal nearly analytic discrete method” (ONADM) for acoustic and elastic equations (Yang *et al.*, 2004), which was an improved version of “nearly analytic discrete method (NADM)” (Yang *et al.*, 2003a) initially suggested by Konddoh *et al.* (1994) for solving parabolic and hyperbolic equations. The method uses a truncated Taylor expansion with respect to time to analytically approximate the wave displacement and its gradients at grid-points. Meanwhile, it uses the wave displacement and its gradients to determine the high-order space derivatives involved in these truncated Taylor formulae. As shown by the numerical results in our earlier work (Yang *et al.*, 2004), the method is very efficient in large-scale seismogram synthetics because it can effectively suppress the numerical dispersion

caused by discretizing the wave equation by using the local interpolation compensation for the truncated Taylor series, while the conventional FD schemes with 2- and 4-order accuracies suffer from numerical dispersion near large velocity contrast or when too few samples per wavelength are used (Fei & Larner, 1995; Yang *et al*., 2002). The efficient synthetics together with algorithms for waveform inversion can help us better understand the earth structure.

The numerical tests reported in the cited reference (Yang *et al.*, 2004) were done in a homogeneous medium. However, most seismologists employ the heterogeneous model to investigate wave propagation as the actual earth is highly heterogeneous. Therefore, it is necessary to examine the proposed algorithm for heterogeneous models. On the other hand, to keep numerical calculations stable and accurate, we typically require the scheme to have certain properties. The stability criterion of a numerical method is crucial in numerically synthetic seismograms, as it can affect the efficiency and performance of the method. A suitable choice of space and time increments guided by the stability criteria can improve the practical computational costs and suppress numerical dispersion, because the numerical dispersions of numerical methods are related to the so-called Courant number which is closely associated with the stability criteria. In the present paper, we investigate the stability condition of the ONADM, which can be used to improve the computational efficiency of the algorithm.

We note that as an important issue in numerical seismic simulations, numerical dispersion has been studied by many researchers. Roughly speaking, numerical dispersion is an unphysical phenomenon caused by discretizing the wave equation (Sei & Symes, 1994; Yang *et al*., 2002). Such a phenomenon makes the wave's velocity frequency dependent. A natural idea in dealing with numerical dispersion is to use accurate methods so that dispersion errors will be intrinsically very small. For instance if one uses discrete Fourier transforms then there is no numerical dispersion in space except for the time dispersion (Kosloff & Baysal, 1982; Fornberg, 1987). However, spectral methods suffer from other drawbacks (Mizutani *et al*., 2000). For example, the PSM taking the Fourier transform means that each point interacts with every other point. In some sense, this is unphysical as the interaction in dynamic elasticity is of a local nature. A remedy is to use local operators with high accuracy that are suitable for fast parallel implementation when we develop seismic models and use numerical methods to generate synthetic seismograms. Regarding the factors stated above, the ONADM provides a good choice for suppressing the numerical dispersion due to its nice local property as confirmed in our earlier work (Yang *et al*., 2004). In this paper, we analyze the theoretical dispersion relation of the ONADM so that we can further reduce the numerical dispersion.

The main purpose of this paper is to evaluate the performance of the ONADM for general heterogeneous media, and to analyze the theoretical properties of the ONADM including the stability criteria for 1-D and 2-D cases, dispersion relation, and theoretical error of the ONADM. For comparison, we also discuss the stability criteria and dispersion relations of the so-called L-W schemes or high-order compact schemes with eighth-order and tenth-order accuracies (Dablain, 1986) and the PSM of second-order accuracy in time (Kosloff & Baysal, 1982). Our theoretical analyses show that the

numerical dispersion of the ONADM does not sense to the Courant number compared with the high-order compact schemes and the PSM, its Courant number limit (stability upper bound) is slightly larger than that of the PSM and slightly smaller than that of the tenth-order compact scheme for the 1-D case. Meanwhile, we compare the waveform results computed by the ONADM and the so-called L-W method with tenth-order and fourth-order accuracies for the 1-D case, and the second-order central schemes for 2-D heterogeneous case.

2 Formulation of ONADM

The scalar wave equations in a homogeneous medium may be written

$$\frac{\partial^2 u}{\partial t^2} = c_0^2 \frac{\partial^2 u}{\partial x^2}, \tag{1}$$

for the 1-D case and

$$\frac{\partial^2 u}{\partial t^2} = c_0^2 \left(\frac{\partial^2 u}{\partial x^2} + \frac{\partial^2 u}{\partial z^2}\right), \tag{2}$$

for the 2-D case, where *u* is the displacement and c_0 is the sound velocity. Applying the optimal nearly-analytic discrete approximation (Yang *et al*., 2004) to equation (1), we have

$$U_j^{n+1} = 2U_j^n - U_j^{n-1} + (c_0\Delta t)^2 \left(\frac{\partial^2 U}{\partial x^2}\right)_j^n + \frac{(c_0\Delta t)^4}{12}\left(\frac{\partial^4 U}{\partial x^4}\right)_j^n, \tag{3}$$

where Δt is the time increment and $U = \left(u, \partial u/\partial x\right)^T$. The evaluation of the high-order derivatives in the formula (3) is presented in Appendix A.

Similarly, for equation (2) we have

$$\overline{U}_{i,j}^{n+1} = 2\overline{U}_{i,j}^{n} - \overline{U}_{i,j}^{n-1} + (c_0\Delta t)^2 \left[\left(\frac{\partial^2 \overline{U}}{\partial x^2}\right)_{i,j}^n + \left(\frac{\partial^2 \overline{U}}{\partial z^2}\right)_{i,j}^n\right]$$

$$+ \frac{(c_0\Delta t)^4}{12}\left[\left(\frac{\partial^4 \overline{U}}{\partial x^4}\right)_{i,j}^n + 2\left(\frac{\partial^4 \overline{U}}{\partial x^2 \partial z^2}\right)_{i,j}^n + \left(\frac{\partial^4 \overline{U}}{\partial z^4}\right)_{i,j}^n\right], \tag{4}$$

where $\overline{U} = \left(u, \partial u/\partial x, \partial u/\partial z\right)^T$. For the high-order derivatives included in formula (4), we refer to the Appendix A.

3 Stability Criteria

It is well known that the time increment Δt must be less than or equal to the Courant limit, in order to keep numerical calculation stable. In this section we derive the

stability conditions of the ONADM for 1-D and 2-D cases. Our approach follows the procedure as in (Richtmyer & Morton, 1967) where the authors presented a variety of stability analyses (1967). Through a series of mathematical operations, we obtain the following stability condition for the 1-D homogeneous case (see Appendix B):

$$\Delta t \le \alpha_{\max} \frac{h}{c_0} \approx 0.754 \frac{h}{c_0}. \qquad (5)$$

For comparison and numerical dispersion analysis, we also give the stability conditions of the high-order L-W schemes (Dablain, 1986) for the 1-D case, presented in Table 1.

Table 1. The approximate maximum Courant numbers of different methods for the 1-D case.

Methods	ONADM	PSM	O(4,10) L-W	O(4,8) L-W
$\alpha_{\max}$	0.754	0.6366	0.893	0.929

From Table 1, we see the stability condition of the ONADM is more relaxed compared to that of the PS method, and slightly tighter comparing with those of the L-W methods with accuracy of O(4,10) and O(4, 8).

For the 2-D homogeneous case, the stability condition of the ONADM (4) under this case of $\Delta x = \Delta z = h$ is given by (see Appendix B)

$$\Delta t \le \alpha_{\max} \frac{h}{c_0} \approx 0.527 \frac{h}{c_0}. \qquad (6)$$

The stability condition for a heterogeneous medium cannot be directly determined, but could be approximated by using a local homogeneous method. Our conjecture is that equations (5) and (6) are approximately correct for a heterogeneous medium if the maximal value of the wave velocity c_0.

4 Numerical Dispersion Analysis

In synthetic seismogram, a well-known and major artifact is the numerical dispersion limiting the usefulness of point-wise discretization schemes for the wave equation. Up to now, finite-difference (FD) methods are the most widely used numerical methods for wave propagation problem in seismology. It was observed (Sei & Symes, 1994) that the higher the order of the FD schemes, the less dispersion is experienced by the wave. This motivates us to use high-order FD schemes (e.g. tenth-order method, Dablain, 1986) to reduce the numerical dispersion. However, a higher order FD method requires more floating point operations as it involves generally more grid-points in a direction. The demand of more grids in higher order FD methods prevents the algorithms from efficient parallel implementation and artificial boundary treatment. Therefore, a higher order method is typically not a good choice in synthetic seismogram (Sei & Symes, 1994). Another way of attacking the numerical dispersions is to use the so-called

flux-corrected transport (FCT) technique, which is typically unable to fully recover the lost resolution by the numerical dispersion when the spatial sampling becomes too coarse (Yang *et al.*, 2002). In this section, we investigate the dispersion relation of the ONADM for the 1-D case so that we can further reduce the numerical dispersion depending on the Courant number of the method. For comparison, we also present the dispersion relations of the so-called Lax-Wendroff or high order compact schemes with 8-order, 10-order accuracy, and the PS method.

In the following, we show the numerical results using the dispersion relations (C3) and (C5). The detailed analysis of the dispersion relation of the ONADM and the so-called L-W corrections with different orders (Dablain, 1986) are presented in the Appendix C.

Figures 1 to 4 plot the dispersion relations for the ONADM, spectral method (Kosloff & Baysal, 1982), and the high order L-W schemes with accuracy of O(4,8) and O(4,10) for the 1-D homogeneous wave equation corresponding to different Courant numbers. Figure 1 shows that the numerical velocity of the ONADM gradually approximates the exact wave velocity while the Courant number α increases in the high frequency range. It also shows that at the stability limit ($\alpha = c_0 \Delta t / \Delta x \approx 0.754$), the numerical dispersion is minimal. This suggests that we can minimize the numerical dispersion caused by the ONADM by using the maximum Courant number while the PSM will have the maximal dispersion error (Figure 2) in the same case. Moreover, the change of numerical dispersion corresponding to the change of the Courant number α is not sensitive as compared with the spectral method (Figure 2) and the high order L-W methods with accuracy of O(4,8) and O(4,10) (Figures 3 and 4). The property is useful in practical calculations because it means that we do not need to consider specially the choice of Courant numbers in the stability range. From Figure 2 we observe that the numerical velocity for the PSM (Kosloff & Baysal, 1982) is usually greater than the exact velocity. This shows that the dispersion in the PSM leads the exact signal while the dispersion in the ONADM follows the signal. However, as we observed in Figures 3 and 4, even for a fixed Courant number, the dispersion of the high-order L-W schemes is irregular. It sometimes leads the exact signal, and sometimes follows the signal. This phenomenon indicates that it is hard to choose a suitable Courant number for the high order L-W schemes.

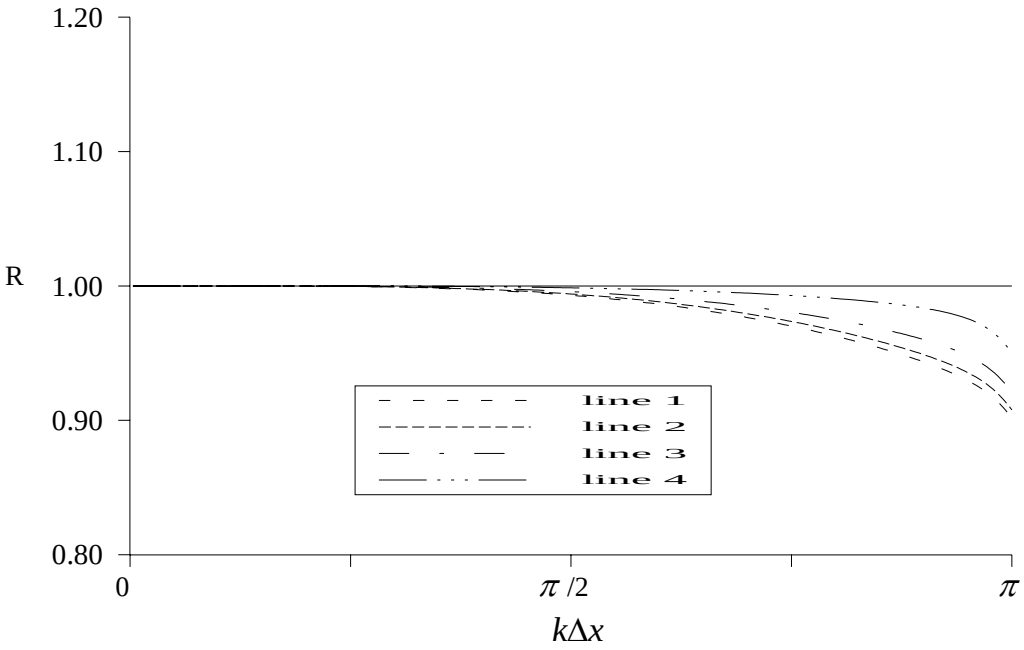

Figure 1. The ratio R_{ONADM} (formula (C3)) of the numerical velocity to the phase velocity versus wavenumber $k\Delta x$ for the ONADM for different Courant numbers $\alpha = c_0 \Delta t / \Delta x$, where lines 1, 2, 3, and 4 correspond to $\alpha = 0.1$, 0.3, 0.5, and $\alpha_{\max}$, respectively.

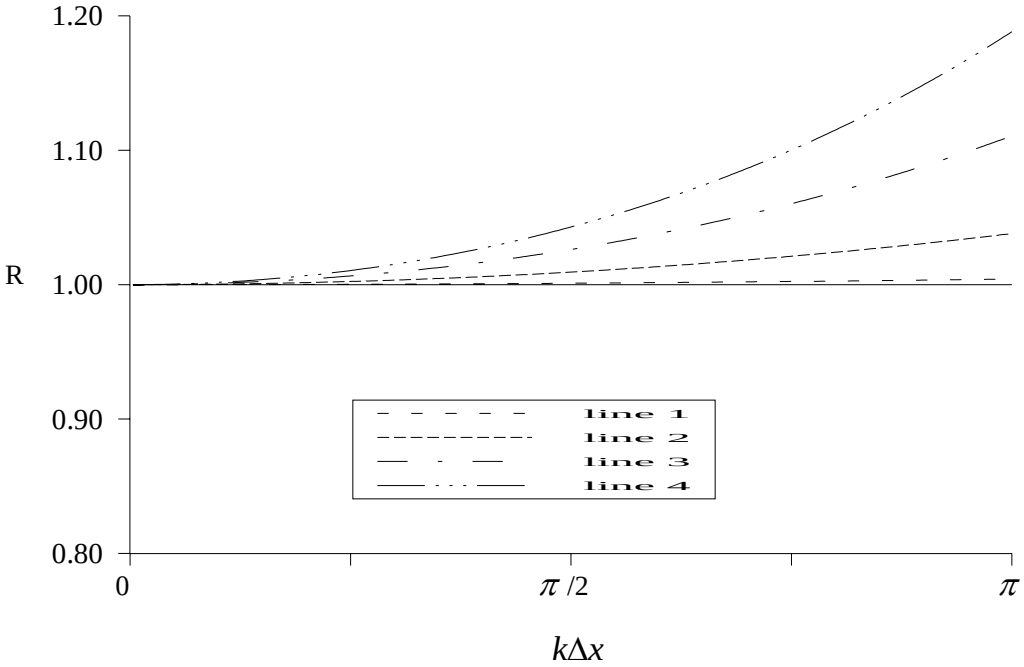

Figure 2. The ratio of the numerical velocity to the phase velocity versus wavenumber $k\Delta x$ for the pseudospectral method (Kosoff and Baysal, 1982) for different Courant numbers $\alpha = c_0 \Delta t / \Delta x$, where lines 1, 2, 3, and 4 correspond to $\alpha = 0.1$, 0.3, 0.5, and

$\alpha_{\max}$, respectively.

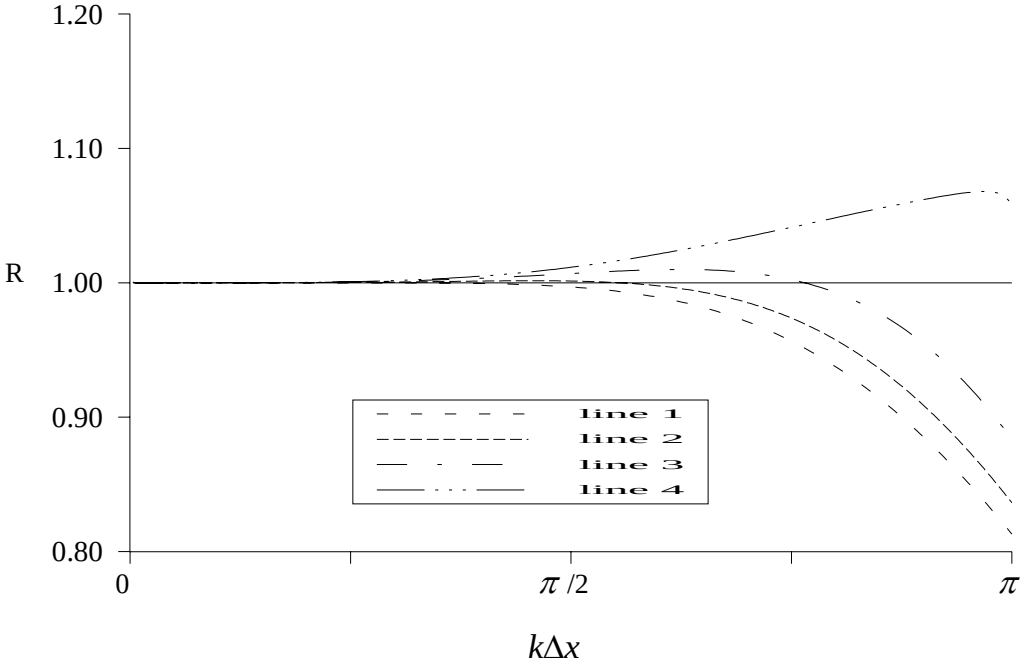

Figure 3. The ratio R_{L-W} (formula (C5)) of the numerical velocity to the phase velocity versus wavenumber $k\Delta x$ for the eighth-order L-W (Dablain, 1986) for different Courant numbers $\alpha = c_0 \Delta t / \Delta x$, where lines 1, 2, 3, and 4 correspond to α =0.1, 0.5, 0.754, and $\alpha_{\max}$, respectively.

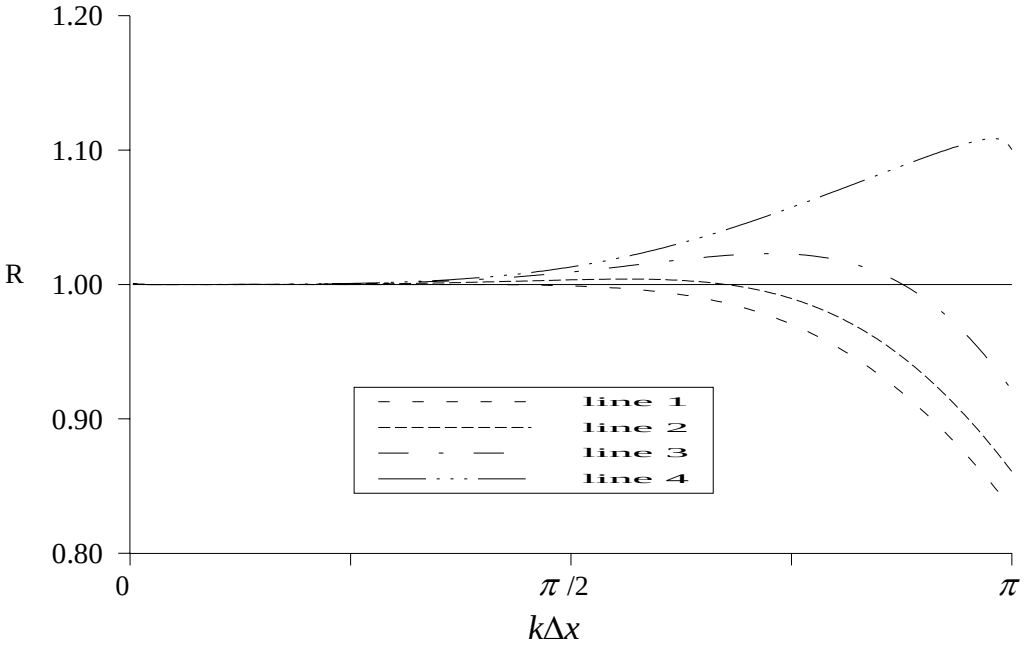

Figure 4. The ratio R_{L-W} (formula (C5)) of the numerical velocity to the phase velocity

versus wavenumber $k\Delta x$ for the tenth-order L-W (Dablain, 1986) for different Courant numbers $\alpha = c_0 \Delta t / \Delta x$, where lines 1, 2, 3, and 4 correspond to $\alpha = 0.1$, 0.5, 0.754, and $\alpha_{\max}$, respectively.

5 Error Analysis

In our earlier work (Yang *et al.*, 2004), we discussed the numeric error of the ONADM. In the present paper we analyze its theoretical error for the scalar wave problem via the Taylor series expansion. For the 1-D case, we have the following theoretical error of the ONADM from equations (D7) and (D9) presented in the Appendix D

$$\begin{aligned} E &= [(D_{2t} - L_{2t}) - (D_{2x} - c_0^2 L_{2x})]U_j^n \\ &= -c_0^2 \left[\frac{(\alpha^4 + 1)\Delta x^4}{360} \left(\frac{\partial^6 u}{\partial x^6} \right)_j^n, \frac{(7\alpha^4 + 3)\Delta x^4}{2520} \left(\frac{\partial^7 u}{\partial x^7} \right)_j^n \right]^T + O(\Delta x^6 + \Delta t^6), \\ &= O(\Delta x^4 + \Delta t^4) \end{aligned} \qquad (7)$$

where D_{2t}, L_{2t}, D_{2x} and L_{2x} are exact derivative and the ONADM difference operators with respect to time and space respectively whose definitions are given in the Appendix D. The detailed derivation of the error E is also presented in the Appendix D, and α is the Courant number defined by $\alpha = c_0 \Delta t / \Delta x$.

For the 2-D case, we have the following theoretical error *E*, derived from equations (D15), (D18), and (D19) as discussed in the Appendix D

$$E = [(D_{2t} - L_{2t}) - (D_{2x} - c_0^2 L_{2x}) - (D_{2z} - c_0^2 L_{2z})]\overline{U}_{i,j}^n = O(\Delta t^4 + \Delta x^4). \qquad (8)$$

These corresponding operators are also defined in the Appendix D.

From the error (7), we see that the error of the ONADM is related to the Courant number α. To demonstrate the effect of the Courant number α on the error of the ONADM, we consider the following 1-D initial problem:

$$\frac{\partial^2 u}{\partial t^2} = c_0^2 \frac{\partial^2 u}{\partial x^2}, \qquad (9a)$$

$$u(0, x) = \cos(-\frac{2\pi f_0}{c_0} \cdot x), \text{ and} \qquad (9b)$$

$$\frac{\partial u(0, x)}{\partial t} = -2\pi f_0 \cdot \sin(-\frac{2\pi f_0}{c_0} \cdot x), \qquad (9c)$$

where f_0 denotes the frequency and c_0 is the wave velocity.

In the numerical example, we choose the grid number N=200, the frequency

f_0=15 Hz, and the wave velocity $c_0 = 6000$ m/sec. The relative error (E_r) is the ratio of the RMS of the residual $(u_i^n - u(t_n, x_i))$ and the RMS of the exact solution $u(t_n, x_i)$. Its explicit definition is as follows:

$$E_r(\%) = \left\{ \frac{1}{\sum_{i=1}^{N} [u(t_n, x_i)]^2} \sum_{i=1}^{N} \left[u_i^n - u(t_n, x_i) \right]^2 \right\}^{\frac{1}{2}} \times 100. \qquad (10)$$

Figure 5 shows the computational results of the relative error E_r at different times, where three lines of E_r corresponding to the Courant numbers of $\alpha = 0.2$ (line 1), 0.5 (line 2), and 0.75 (line 3) are shown in a semi-log scale. Figure 6 plots the relative errors E_r versus Courant numbers at different calculation time t=1.8 s, 1.2 s, and 0.6 s. From Figures 5 and 6, we can conclude that the error introduced by the ONADM measured by E_r tends to decrease as the Courant number increases. It suggests that we can reduce the numerical errors through choosing the maximum Courant number.

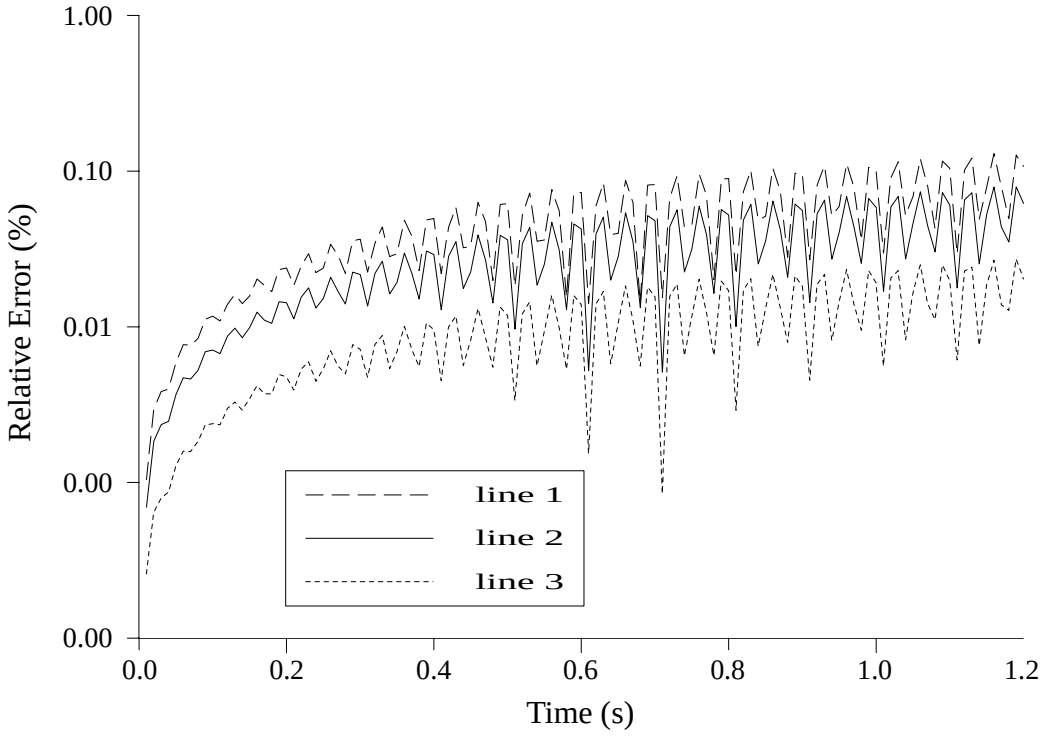

Figure 5. The relative errors of the ONADM measured by E_r are shown in a semi-log scale for the 1-D initial problem (9), where lines 1, 2, and 3 correspond to different Courant numbers $\alpha = 0.2$, 0.5, and 0.75, respectively.

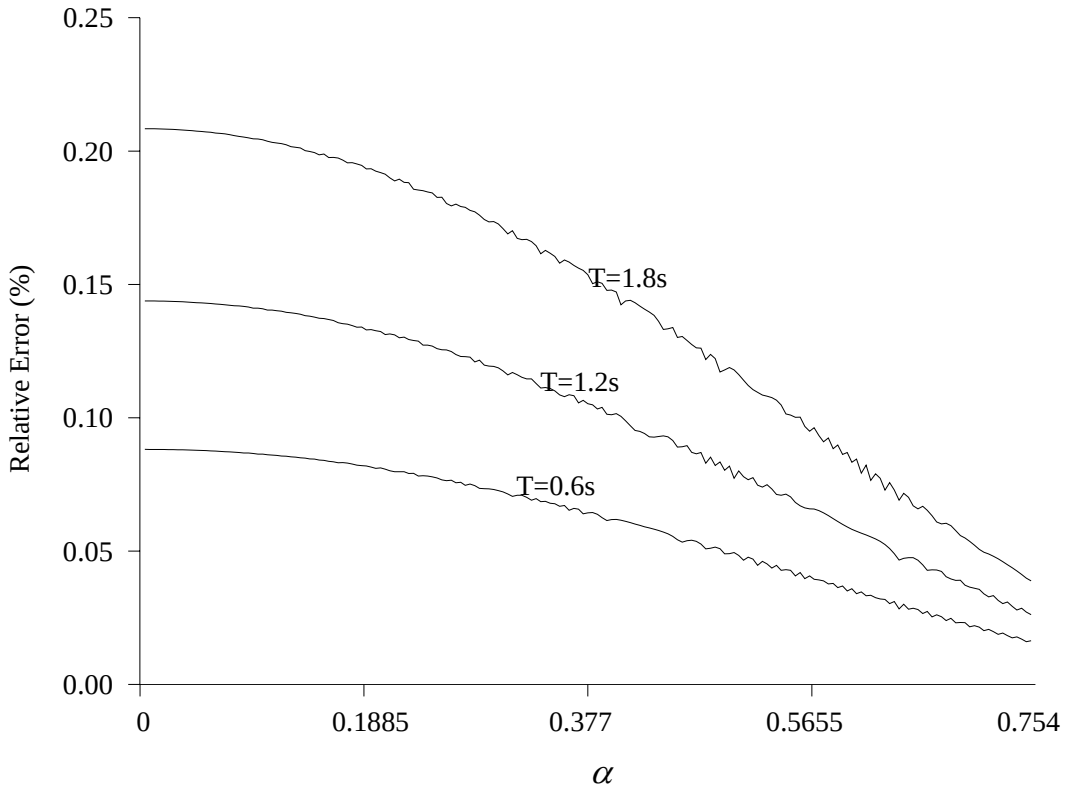

Figure 6. The relative errors of the NADM versus Courant number α, measured by $E_{r,}$ are shown in a semi-log scale for the 1-D initial problem (9), where lines 1, 2, and 3 correspond to different times $T = 0.6$ sec, 1.2 sec, and 1.8 sec, respectively.

6 Numerical Modeling

In this section, we test the ONADM for 2-D heterogeneous isotropic media. To start, we first compare the synthetic seismograms for the 1-D case, computed by the ONADM and the L-W methods with accuracy of O(4, 10) and O(4,4) (Dablain, 1986).

1-D case

The velocity model is selected for our comparative study, as illustrated in Figure 7 (similar to Dablain's model, 1986). The distance from the source to the farthest receiver is 5.28 *km*. The total model is 10.4 *km* long. The source is an explosive source that is at coordinate $z_s = 2.6$ *km* and has a Ricker wavelet with a peak frequency of f_0=20 Hz. The time variation of the source function is $\sin(2\pi f_0 t)\exp(-4\pi^2 f_0^2 t^2 / 16)$. The receiver positions are located at $z_s = 3.9$ *km*, 6.5 *km*, and 7.8 *km*, respectively. Other parameters are chosen as the minimum velocity: 2500 m/s, the maximum velocity: 3700 m/s, the

spatial increment $\Delta x = 10$ *m*, and the time increment $\Delta t = 0.002$ s resulting in the maximum Courant number $\overline{\alpha}_{\max} = c_{\max} \Delta t / \Delta x = 0.74$. Total data length is 2.4 s.

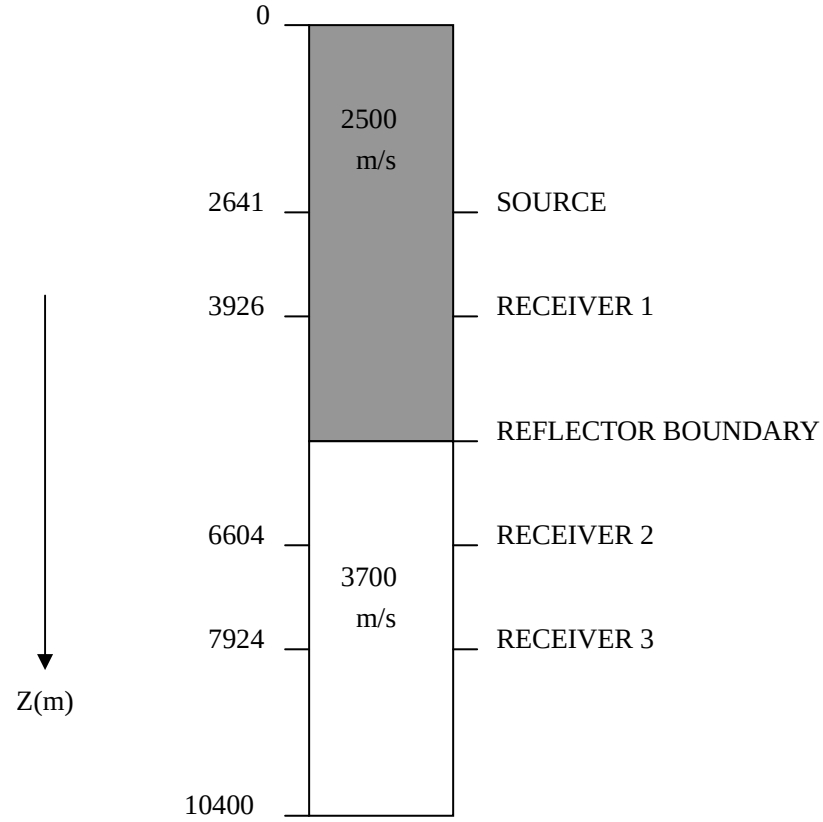

Figure 7. 1-D model for comparisons between the ONADM and the high-order L-W methods.

Figures 8, 9, and 10 show the primary arrivals at receivers 1, 2, and 3, computed by the ONADM, the O(4,10) and O(4,4) L-W methods, respectively. Figures 8 and 9 show that the waveforms generated by the ONADM are identical with those computed by the O(4,10) L-W scheme excepting for marginal difference near wave peaks, while the O(4,4) L-W scheme suffers from seriously numerical dispersions (see Figure 10). This verifies the convergence of the ONADM because the convergence of the O(4,10) L-W scheme was demonstrated and equivalent with the PSM in Dablain's study (Dablain, 1986). In Figure 9, we can also see the anomalous dispersion leading the exact signal, which is the same as that caused by the PSM (Dablain, 1986).

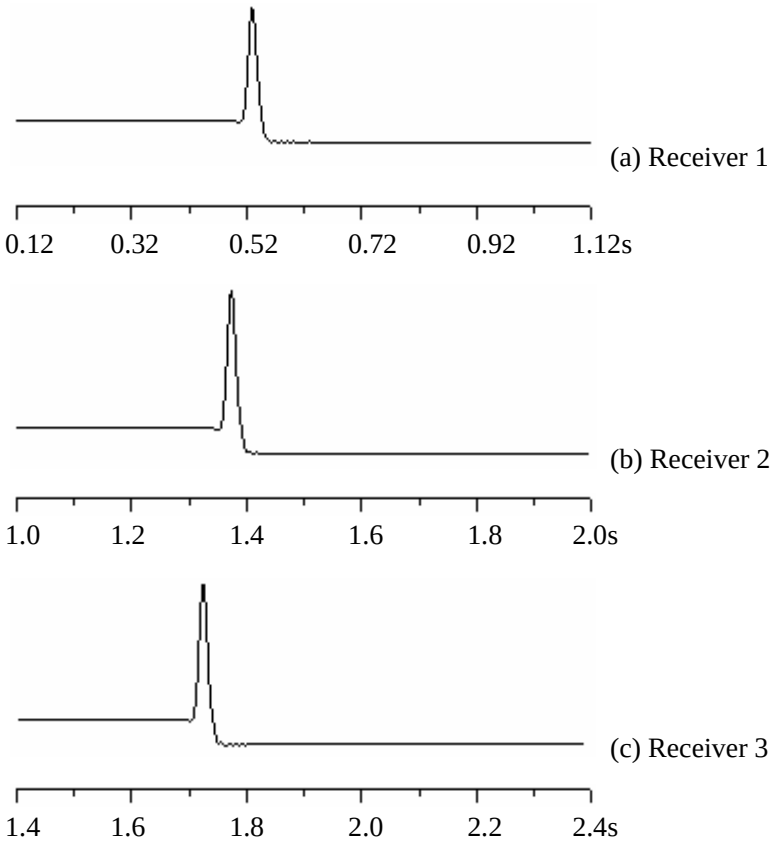

Figure 8. The waveforms generated by the ONADM for the 1-D case.

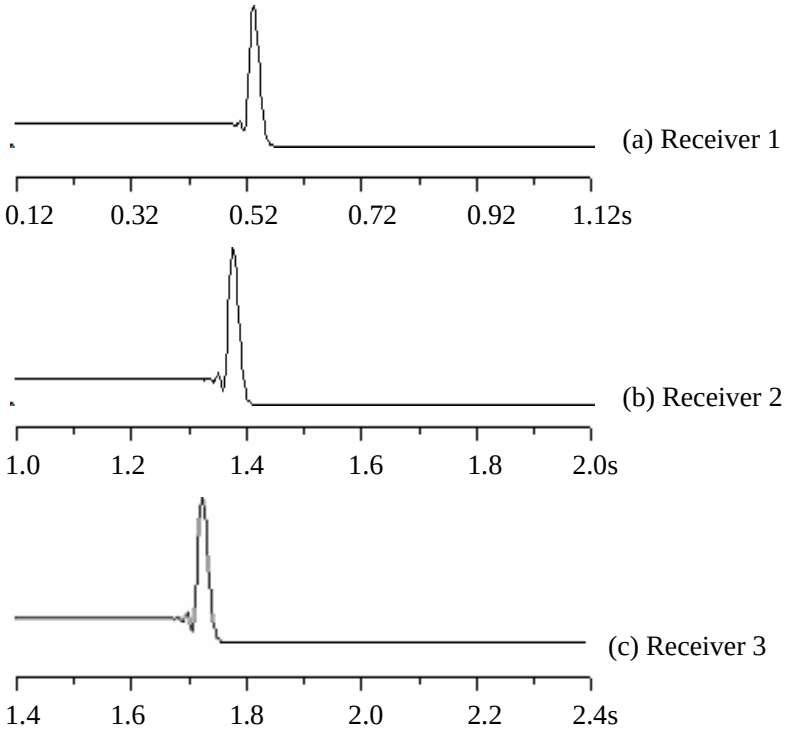

Figure 9. The waveforms generated by the O(4, 10) L-W method (Dablain, 1986) for the 1-D case.

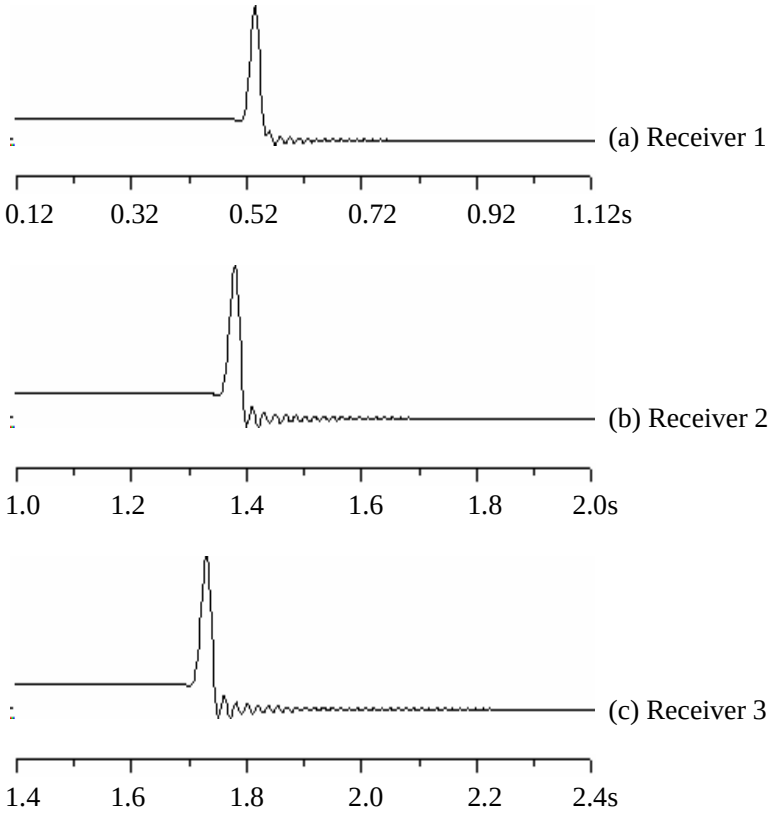

Figure 10. The waveforms generated by the O(4, 4) L-W method (Dablain, 1986) for the 1-D case.

2-D heterogeneous case

To demonstrate the performance of the ONADM in 2-D heterogeneous case, we choose three models for testing. In our experiments, the 2-D heterogeneous wave equation is

$$\frac{\partial^2 u}{\partial t^2} = \frac{1}{\rho(x,z)}\left[\frac{\partial}{\partial x}\left(\mu(x,z)\frac{\partial u}{\partial x}\right)+\frac{\partial}{\partial z}\left(\mu(x,z)\frac{\partial u}{\partial z}\right)\right]+\frac{f}{\rho(x,z)}, \qquad (11)$$

where $\rho(x,z)$ is the density, $\mu(x,z)$ is the elastic parameter, f is the source function with the same time variation function as that of the 1-D case in the following numerical experiments.

Model 1 In our first example, we choose the model of two-layer media with the curve inner interface governed by the following depth function

$$z = 1+\frac{1}{2}\left(1+\sin\frac{2\pi(7.5-x)}{10}\right),\ \ 0\le x\le 10 \ \ km.$$

The medium model was shown in Figure 11, where the medium parameters are chosen by:

$\mu_1(x,z)=25.4$ GPa, $\rho_1(x,z)=1.8g/cm^3$, $\mu_2(x,z)=26.672$ GPa,

$\rho_2(x,z) = 3.0g/cm^3$, corresponding to the top (subscript 1) and bottom (subscript 2) layers, respectively. The computational domain is $0 \le x \le 10$ km, $0 \le z \le 3$ km. We choose the spatial increment *h*=20 m, the time increment $\Delta t = 2\times10^{-3}$ sec, and the number of grid points 501×151. The source is an explosive source that is at coordinate (x_s, z_s) =(0.06 km, 5 km) and has a Ricker wavelet with a peak frequency of f_0=15 Hz. The wavefields are recorded by 501 receivers on the surface spread from *x*=0 to *x*=10 km spaced 0.02 km apart.

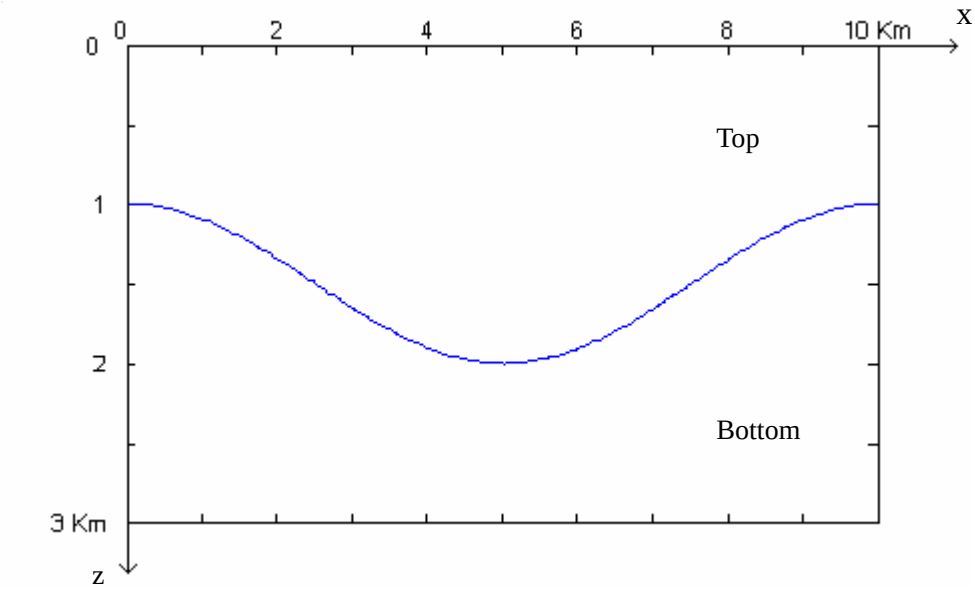

Figure 11. 2-D medium model with an inner curve interface.

Figures 12 and 13 are the synthetic seismograms generated by the ONADM. In Figure 12 the reflected waves from the curve inner interface and the free surface are very clear. We can identify clearly the structure of medium from the reflected curve wave shown in Figure 12 for the chosen medium model. But when we choose the density $\rho_2(x,z) = 2.0g/cm^3$ and keep other parameters the same as in the synthetic seismogram shown in Figure 12, we can not see the reflected curve wave from Figure 13. The computation to generate the synthetic seismograms in Figures 12 and 13 was done on a Pentium 4 PC with 256MB RAM. It took about 6 min for the model 1. In this numerical experiment, we use the 4-times absorbing boundary condition developed by Higdon (1991) and discretized by Yang *et al*. (2003b) based on the stable biased-center scheme.

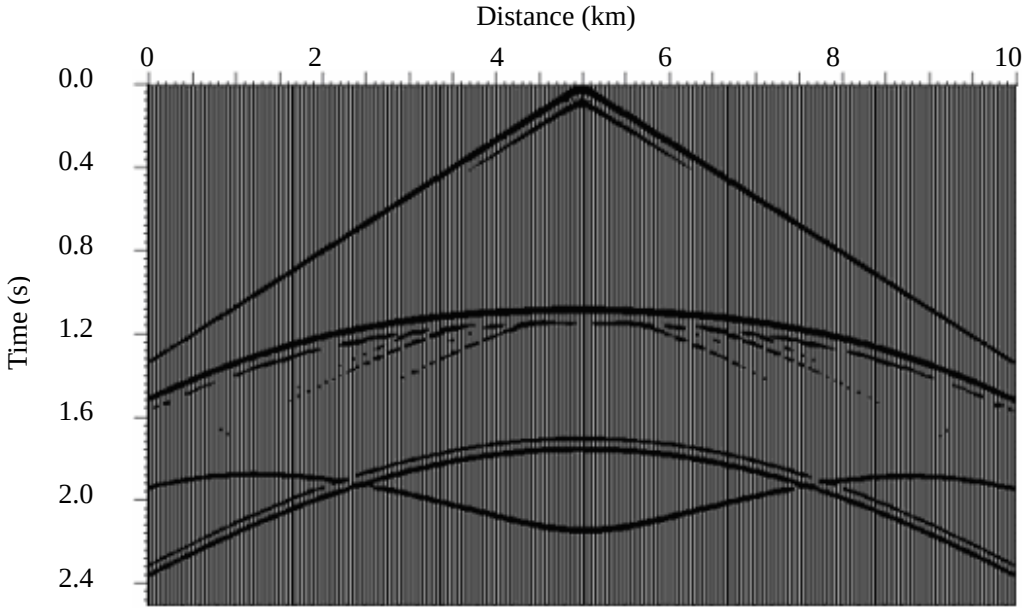

Figure 12. The synthetic seismogram on the surface, generated by the ONADM for the 2-D model 1 with $\rho_2(x,z) = 3.0g/cm^3$ shown Figure 11.

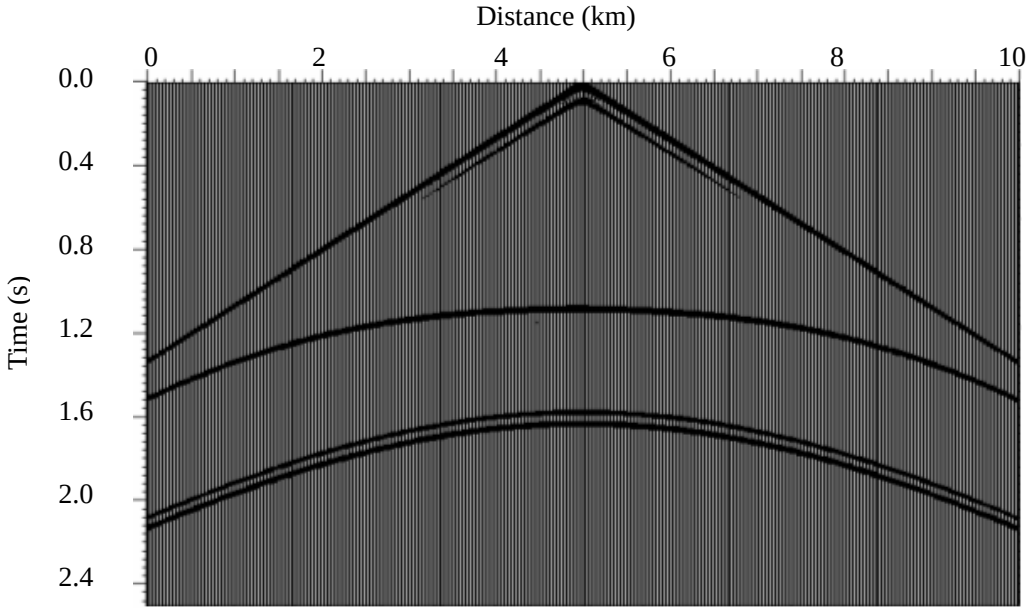

Figure 13. The synthetic seismogram on the surface, generated by the ONADM for the 2-D model 1 with $\rho_2(x,z) = 2.0g/cm^3$ shown Figure 11.

Model 2 In this experiment, we compare the performances of the ONADM and the second order FD method for the complete heterogeneous problem. For this case, we consider a two-layer heterogeneous medium whose density and elastic parameters are as follows:

$$\rho(x,z) = \rho_0 * (1 + \frac{x}{50}),$$

$$\mu(x,z) = 16 + \frac{x}{4} + \frac{z}{2},$$

where the constant density ρ_0 equals to 2.1 g/cm^3 and 3.0 g/cm^3 for the upper and bottom layers, respectively. The horizontal inner interface is located at the depth z=3.924 km.

In the example, The computational domain is chosen as $0 \le x \le 6.048$ km, $0 \le z \le 6.048$ km. The source is an explosive source that is at coordinate $(x_s, z_s) = (3.024$ km, 3.024 km) and has a Ricker wavelet with a peak frequency of f_0=15 Hz. The time variation of the source is the same as that in the 1-D case. Three receivers are at $(x_1, z_1) = (4.464$ km, 1.404 km), $(x_2, z_2) = (4.464$ km, 1.764 km), and $(x_3, z_3) = (4.464$ km, 2.124 km).

The waveforms, generated by the ONADM and the second-order central FD method (Kelly *et al.*, 1976), are compared in Figures 14 and 15. The coarse spatial step in the ONADM computations is chosen by *h*=36 *m*. The time increment is $\Delta t = 4.6 \times 10^{-3}$ sec. To generate Figure 15, the fine-grid step is chosen by *h*=6 m, the time increment is chosen by $\Delta t = 1.15 \times 10^{-3}$ sec resulting in that the Courant number is about 1.5 times of that used in the ONADM calculation. Figures 14 and 15 show that the waveforms generated by the ONADM on the coarse grids are identical with those computed by the second-order FD method on the fine grids excepting for slight difference behind the main wave peak. The difference is mainly caused by the numerical dispersions and the source-generated noises (artifacts due to source location at grid points). But from Figure 14 we can observe that the ONADM has fairly less numerical dispersions when the coarse-grid step is used. It indicates that the ONADM enables wave propagation to be simulated in large-scale heterogeneous models through using the coarse computation grids. There is a significant difference between the efficiency of the FD and the ONADM. It took the ONADM about 45 seconds CPU time to generate Figure 14, while generating Figure 15 under the same computer environments costs the second-order FD about 14 minutes. The required storage for the FD method is about 12 times of that for the ONADM.

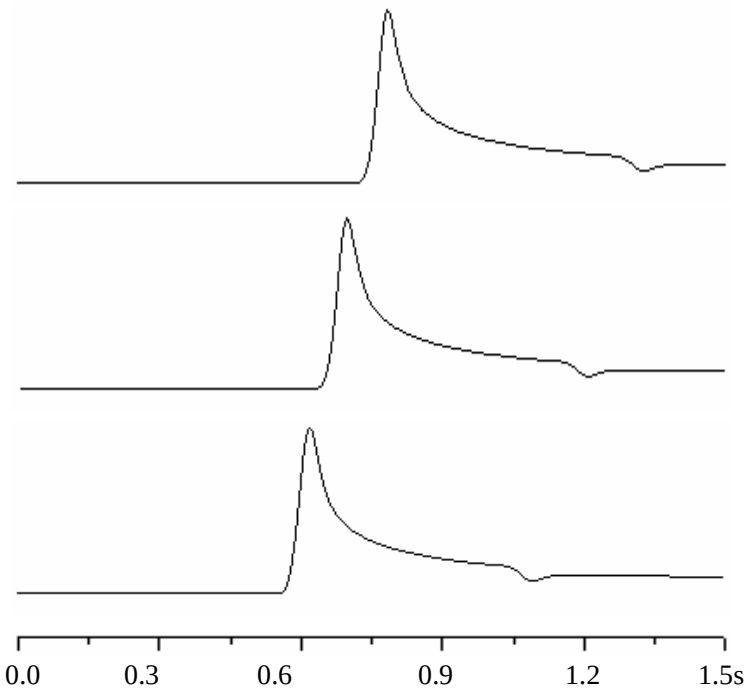

Figure 14. The waveforms generated by the ONADM for the 2-D heterogeneous model 2.

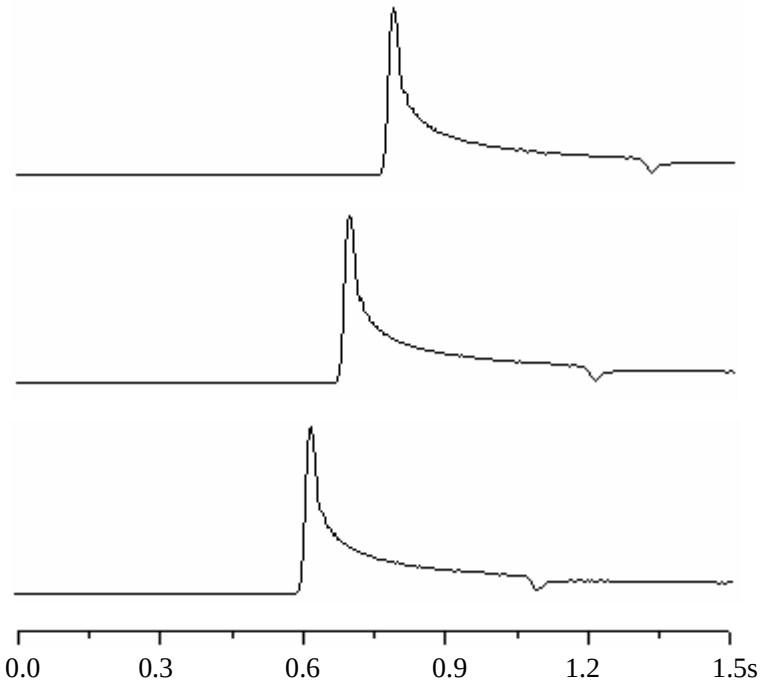

Figure 15. The waveforms generated by the second-order FD method (Kelly *et al*., 1976) for the 2-D heterogeneous model 2.

Model 3 To investigate the performance of the ONADM for the large heterogeneous model, we choose the computational domain as $0 \le x \le 16$ km, $0 \le z \le 16$ km, and the number of grid points 401×401. The source is located at the center of the computational domain and the horizontal inner interface is at z=9.4 *km*. The spatial and time increments are *h*=40 *m* and $\Delta t = 6.7 \times 10^{-3}$ sec so that the maximum value of the Courant number α is about 0.526. The rest parameters are the same as those used in model 2.

Figure 16 is the wave-field snapshot at t=2.5 sec generated by the ONADM. From the wave-field snapshot, we can clearly observe that the reflection of the acoustic-wave from the inner interface, and the computation is stable for the Courant number 0.526 that nears to the maximum Courant number of keeping the ONADM stable. The wave-field snapshot also shows that the ONADM has less numerical dispersions even if the space increment chosen is 40 m without any additional treatments. The computation to generate the wave-field snapshot in Figure 16 was done on a Pentium 4 PC with 256MB RAM. The ONADM took about 7 min to finish the job.

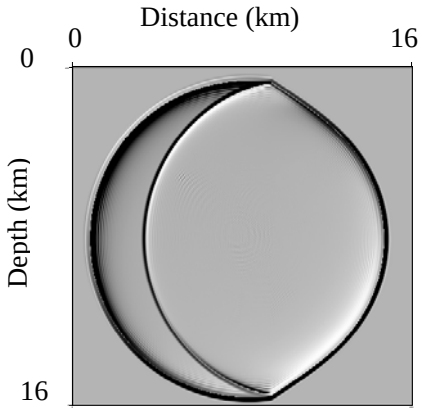

Figure 16. Snapshot of seismic wave fields at time 2.5 sec in heterogeneous isotropic media, generated by the ONADM.

7 Conclusions

We analyze theoretically that the ONADM has 4-order accuracy in both space and time, and give the stability conditions of the ONADM for 1-D and 2-D case when it is applied to the scalar wave equation. Numerical calculations under the cases of large Courant numbers for 1-D and 2-D problems demonstrate the efficiency of the stability conditions obtained in our present study. Numerical dispersion analysis shows that we can minimize the numerical dispersion through using the optimal Courant number that approximately equals to the maximum Courant number $\alpha_{\max}$ for the ONADM. The grid dispersion of the ONADM lessens with increasing the Courant number α, and the numerical dispersion is minimal as the Courant number α equals to the stability limit

$\alpha_{\max} \approx 0.754$ for the 1-D case. Generally speaking, the grid dispersion of the ONADM is smaller than those of the high-order compact or so-called L-W schemes with accuracy of O(4, 8) and O(4, 10) (Dablain, 1986) in the high frequency range, the maximum numerical error of the ONADM decreases as the Courant number increases.

This study also indicates that the ONADM can be directly applied to the heterogeneous case without any additional treatments because the gradients of the wave displacement is simultaneously computed in the ONADM, while the so-called L-W schemes (Dablain, 1986) can be not directly applied the heterogeneous problem because equation (11) may involve the displacement gradients. Synthetic seismograms generated by the ONADM for the heterogeneous problem illustrate that the ONADM can effectively suppress numerical dispersions and source noises when too-coarse computation grids are used. This further demonstrates that the ONADM enables wave propagation in heterogeneous media to be simulated in large-scale models through using the coarse computation grids.

Appendix A: Evaluation of the High-Order Derivatives

To apply the optimal scheme (3) to compute the values of *U* at time t_{n+1} in synthetic seismograms, we need the high-order derivatives including equation (3). To determine the high-order derivatives, following the "analysis thought" (Konddoh *et al*., 1994), we use the following interpolation function of the spatial step Δx

$$G(\Delta x) = \sum_{r=0}^{5} \frac{1}{r!} (\Delta x \frac{\partial}{\partial x})^r u, \tag{A1}$$

and construct the following connection relations

$$[G(-\Delta x)]_i^n = u_{i-1}^n, \quad [G(\Delta x)]_i^n = u_{i+1}^n, \tag{A2}$$

$$\left[\frac{\partial}{\partial \Delta x} G(-\Delta x)\right]_i^n = \left(\frac{\partial u}{\partial x}\right)_{i-1}^n, \text{ and } \left[\frac{\partial}{\partial \Delta x} G(\Delta x)\right]_i^n = \left(\frac{\partial u}{\partial x}\right)_{i+1}^n. \tag{A3}$$

Using the relations (A2) and (A3), we can determine the high-order derivatives expressed by the displacement and its gradient. For convenience, we give the approximation formulae as follows

$$\partial_{2x} u_j^n = \frac{2}{\Delta x^2} \delta_x^2 u_j^n - \frac{1}{2\Delta x} \left(E_x^1 - E_x^{-1}\right) \partial_x u_j^n, \tag{A4}$$

$$\partial_{3x} u_j^n = \frac{15}{\Delta x^3} \left(E_x^1 - E_x^{-1}\right) u_j^n - \frac{3}{2\Delta x^2} \left(E_x^1 + 8I + E_x^{-1}\right) \partial_x u_j^n, \tag{A5}$$

$$\partial_{4x} u_j^n = \frac{12}{\Delta x^4} \delta_x^2 u_j^n - \frac{6}{\Delta x^3} \left(E_x^1 - E_x^{-1}\right) \partial_x u_j^n, \tag{A6}$$

$$\partial_{5x}u_j^n = \frac{90}{\Delta x^5}\left(E_x^1 - E_x^{-1}\right)u_j^n - \frac{30}{\Delta x^4}\left(E_x^1 + 4I + E_x^{-1}\right)\partial_x u_j^n, \tag{A7}$$

where $\partial_{mx}u_j^n = \left(\partial^m u/\partial x^m\right)_j^n$, I is a unchangeable operator. δ_x^2 and E_x are the second central difference and displacement operators defined by

$$\delta_x^2 u_j^n = u_{j+1}^n - 2u_j^n + u_{j-1}^n,\ E_x^1 u_j^n = u_{j+1}^n, \text{ and } E_x^{-1}u_j^n = u_{j-1}^n.$$

Similarly, following the "analysis thought" (Konddoh *et al*., 1994) and the original NADM (Yang *et al.*, 2003a), for the 2-D acoustic case the approximation formulae of determining the high-order derivatives can be written as follows

$$\partial_{2x}u_{i,j}^n = \frac{2}{\Delta x^2}\delta_x^2 u_{i,j}^n - \frac{1}{2\Delta x}(E_x^1 - E_x^{-1})\partial_x u_{i,j}^n, \tag{A8}$$

$$\partial_{2z}u_{i,j}^n = \frac{2}{\Delta z^2}\delta_z^2 u_{i,j}^n - \frac{1}{2\Delta z}(E_z^1 - E_z^{-1})\partial_z u_{i,j}^n, \tag{A9}$$

$$\partial_{3x}u_{i,j}^n = \frac{15}{\Delta x^3}(E_x^1 - E_x^{-1})u_{i,j}^n - \frac{3}{2\Delta x^2}(E_x^1 + 8I + E_x^{-1})\partial_x u_{i,j}^n, \tag{A10}$$

$$\partial_{3z}u_{i,j}^n = \frac{15}{\Delta z^3}(E_z^1 - E_z^{-1})u_{i,j}^n - \frac{3}{2\Delta z^2}(E_z^1 + 8I + E_z^{-1})\partial_z u_{i,j}^n, \tag{A11}$$

$$\begin{aligned}\partial_{2xz}u_{i,j}^n = {} & \frac{1}{4\Delta x^2\Delta z}\left(5E_x^1E_z^1 - 5E_x^{-1}E_z^{-1} + E_x^1E_z^{-1} - E_x^{-1}E_z^1 - 4E_z^1 + 4E_z^{-1} - 6E_x^1 + 6E_x^{-1}\right)u_{i,j}^n \\ & - \frac{1}{2\Delta x\Delta z}[-E_x^1E_z^1 - E_x^{-1}E_z^{-1} + E_z^1 + E_z^{-1} - 2\delta_x^2)\partial_x u_{i,j}^n + \frac{1}{\Delta x^2}\delta_x^2(\partial_z u_{i,j}^n)\end{aligned} \tag{A12}$$

$$\begin{aligned}\partial_{x2z}u_{i,j}^n = {} & \frac{1}{4\Delta x\Delta z^2}\left(5E_x^1E_z^1 - 5E_x^{-1}E_z^{-1} - E_x^1E_z^{-1} + E_x^{-1}E_z^1 - 4E_x^1 + 4E_x^{-1} - 6E_z^1 + 6E_z^{-1}\right)u_{i,j}^n \\ & - \frac{1}{2\Delta x\Delta z}[-E_x^1E_z^1 - E_x^{-1}E_z^{-1} + E_x^1 + E_x^{-1} - 2\delta_x^2)\partial_z u_{i,j}^n + \frac{1}{\Delta z^2}\delta_z^2(\partial_x u_{i,j}^n)\end{aligned} \tag{A13}$$

$$\partial_{4x}u_{i,j}^n = -\frac{12}{\Delta x^4}\delta_x^2 u_{i,j}^n + \frac{6}{\Delta x^3}(E_x^1 - E_x^{-1})\partial_x u_{i,j}^n, \tag{A14}$$

$$\partial_{4z}u_{i,j}^n = -\frac{12}{\Delta z^4}\delta_z^2 u_{i,j}^n + \frac{6}{\Delta z^3}(E_z^1 - E_z^{-1})\partial_z u_{i,j}^n, \tag{A15}$$

$$\partial_{2x2z}u_{i,j}^n = \frac{1}{\Delta x^2\Delta z^2}\left(E_x^1E_z^1 + E_x^{-1}E_z^{-1} + E_x^{-1}E_z^1 + E_x^1E_z^{-1} - 2\delta_x^2 - 2E_z^1 - 2E_z^{-1}\right)u_{i,j}^n, \tag{A16}$$

$$\partial_{5x}u_{i,j}^{n} = -\frac{90}{\Delta x^{5}}(E_{x}^{1} - E_{x}^{-1})u_{i,j}^{n} + \frac{30}{\Delta x^{4}}(E_{x}^{1} + 4I + E_{x}^{-1})\partial_{x}u_{i,j}^{n}, \tag{A17}$$

$$\partial_{5z}u_{i,j}^{n} = -\frac{90}{\Delta z^{5}}(E_{z}^{1} - E_{z}^{-1})u_{i,j}^{n} + \frac{30}{\Delta z^{4}}(E_{z}^{1} + 4I + E_{z}^{-1})\partial_{z}u_{i,j}^{n}, \tag{A18}$$

$$\partial_{4xz}u_{i,j}^{n} = \frac{-3}{\Delta x^{4}\Delta z}\left(5E_{x}^{1}E_{z}^{1} - 5E_{x}^{-1}E_{z}^{-1} + E_{x}^{1}E_{z}^{-1} - E_{x}^{-1}E_{z}^{1} - 4E_{z}^{1} + 4E_{z}^{-1} - 6E_{x}^{1} + 6E_{x}^{-1}\right)u_{i,j}^{n} + \frac{6}{\Delta x^{3}\Delta z}[E_{x}^{1}E_{z}^{1} + E_{x}^{-1}E_{z}^{-1} + 2\delta_{z}^{2} - E_{x}^{1} - E_{x}^{-1})\partial_{x}u_{i,j}^{n} \tag{A19}$$

$$\partial_{x4z}u_{i,j}^{n} = \frac{-3}{\Delta x\Delta z^{4}}\left(5E_{x}^{1}E_{z}^{1} - 5E_{x}^{-1}E_{z}^{-1} - E_{x}^{1}E_{z}^{-1} + E_{x}^{-1}E_{z}^{1} - 4E_{x}^{1} + 4E_{x}^{-1} - 6E_{z}^{1} + 6E_{z}^{-1}\right)u_{i,j}^{n} + \frac{6}{\Delta x\Delta z^{3}}[E_{x}^{1}E_{z}^{1} + E_{x}^{-1}E_{z}^{-1} + 2\delta_{x}^{2} - E_{z}^{1} - E_{z}^{-1})\partial_{z}u_{i,j}^{n} \tag{A20}$$

$$\partial_{3x2z}u_{i,j}^{n} = \frac{3}{\Delta x^{3}\Delta z^{2}}\left(E_{x}^{1}E_{z}^{1} - E_{x}^{-1}E_{z}^{-1} + E_{x}^{1}E_{z}^{-1} - E_{x}^{-1}E_{z}^{1} - 2E_{x}^{1} + 2E_{x}^{-1}\right)u_{i,j}^{n} - \frac{6}{\Delta x^{2}\Delta z^{2}}\delta_{z}^{2}(\partial_{x}u_{i,j}^{n}), \tag{A21}$$

$$\partial_{2x3z}u_{i,j}^{n} = \frac{3}{\Delta x^{2}\Delta z^{3}}\left(E_{x}^{1}E_{z}^{1} - E_{x}^{-1}E_{z}^{-1} + E_{x}^{-1}E_{z}^{1} - E_{x}^{1}E_{z}^{-1} - 2E_{z}^{1} + 2E_{z}^{-1}\right)u_{i,j}^{n} - \frac{6}{\Delta x^{2}\Delta z^{2}}\delta_{x}^{2}(\partial_{z}u_{i,j}^{n}), \tag{A22}$$

where $\partial_{mxkz}u_{i,j}^{n} = \left(\partial^{m+k}u/\partial x^{m}\partial z^{k}\right)_{i,j}^{n}$, and these notations in equations (A8) to (A22) denote the same significance as those presented in equations (A3) to (A7). For example, δ_{z}^{2} and E_{z} are the second central difference and displacement operators in the z-direction, which are defined by

$\delta_{z}^{2}u_{i,j}^{n} = u_{i,j+1}^{n} - 2u_{i,j}^{n} + u_{i,j-1}^{n}$, $E_{z}^{1}u_{i,j}^{n} = u_{i,j+1}^{n}$, and $E_{z}^{-1}u_{i,j}^{n} = u_{i,j-1}^{n}$.

Appendix B: Derivation of the stability criteria

1-D homogeneous case

To obtain the stability conditions, we consider harmonic solutions of equation (3). Substituting the solution

$$U_{j}^{n} = \begin{pmatrix} u \\ v \end{pmatrix}^{n} \exp(i(kjh)), \tag{B1}$$

into equation (3) with relations (A4) to (A7), we obtain the following equation

$$(u^{n+1}, \bar{u}^{n+1}, v^{n+1}, \bar{v}^{n+1})^T = A(u^n, \bar{u}^n, v^n, \bar{v}^n)^T, \tag{B2}$$

where k is the wavenumber, $v = \partial u / \partial x$, $\bar{u}^n = u^{n-1}$, and $\bar{v}^n = v^{n-1}$. The matrix A in equation (B2) is given by

$$A = \begin{bmatrix} 2-2a_1 & -ib_1 & -1 & 0 \\ ia_2 & 2-2b_2 & 0 & -1 \\ 1 & 0 & 0 & 0 \\ 0 & 1 & 0 & 0 \end{bmatrix} \tag{B3}$$

where

$$a_1 = \alpha^2(-2+\alpha^2)(\cos(kh)-1),$$

$$a_2 = 15\alpha^2(1-\alpha^2)\sin(kh)/h,$$

$$b_1 = c_0\Delta t\alpha(1-\alpha^2)\sin(kh),$$

$$b_2 = \alpha^2[3(\cos(kh)+4) - 5\alpha^2(\cos(kh)+2)],$$

and the Courant number is defined by $\alpha = c_0\Delta t / h$ with $h = \Delta x$.

From the matrix A we can obtain numerically the following stability condition via solving the eigenvalues of satisfying $|\lambda(A)| \le 1$ of the matrix A

$$\alpha \le \alpha_{\max} \approx 0.754, \tag{B4}$$

or

$$\Delta t \le \alpha_{\max}\frac{h}{c_0} \approx 0.754\frac{h}{c_0},$$

where $\alpha_{\max}$ denotes the maximum Courant number which keeps the numerical calculation stable.

2-D homogeneous case

For the 2-D problem, we consider the case of $\Delta x = \Delta z = h$. Under the case of our consideration the derivation follows the same steps as in the 1-D case. Substituting the following plane-wave solution

$$\bar{U}^n_{m,j} = \bar{U}^n \exp(i(k_x mh + k_z jh)), \tag{B5}$$

into equation (4) with relations (A8) to (A22), we obtain the following equation

$$\bar{U}^{n+1} = B\bar{U}^n, \tag{B6}$$

in which

$$B=\begin{bmatrix} 2-2a_1 & i\Delta t c_0 b_1 & i\Delta t c_0 c_1 & -1 & 0 & 0 \\ \frac{i}{h}a_2 & 2-2b_2 & c_2 & 0 & -1 & 0 \\ \frac{i}{h}a_3 & b_3 & 2-2c_3 & 0 & 0 & -1 \\ 1 & 0 & 0 & 0 & 0 & 0 \\ 0 & 1 & 0 & 0 & 0 & 0 \\ 0 & 0 & 1 & 0 & 0 & 0 \end{bmatrix}$$

where

$$a_1 = 2(2-\cos\theta_1-\cos\theta_2)\alpha^2-(7+\cos\theta_1\cos\theta_2-4\cos\theta_1-4\cos\theta_2)\alpha^4/3,$$

$$b_1 = -\alpha(1-\alpha^2)\sin\theta_1,$$

$$c_1 = -\alpha(1-\alpha^2)\sin\theta_2,$$

$$a_2 = (13\cos\theta_1-\sin\theta_2+2\sin\theta_1\cos\theta_2+3\cos\theta_1\sin\theta_2)\alpha^2+ (-3\cos\theta_1\sin\theta_2-15\sin\theta_1+3\sin\theta_2)\alpha^4,$$

$$b_2 = (7+1.5\cos\theta_1-\cos\theta_2)\alpha^2-(6+2.5\cos\theta_1-\cos\theta_2)\alpha^4$$

$$c_2 = (2+\cos\theta_2-2\cos\theta_1-\cos(\theta_1+\theta_2))\alpha^2-(\cos(\theta_1+\theta_2)+2\cos\theta_1-\cos\theta_2-2)\alpha^4,$$

$$a_3 = (13\sin\theta_2-3\sin\theta_1+3\sin\theta_1\cos\theta_2+2\cos\theta_1\sin\theta_2)\alpha^2+ (-3\sin\theta_1\cos\theta_2+3\sin\theta_1-15\sin\theta_2)\alpha^4,$$

$$b_3 = (2+\cos\theta_1-2\cos\theta_2-\cos(\theta_1+\theta_2))\alpha^2-(2+\cos\theta_1-\cos(\theta_1+\theta_2)-2\cos\theta_2)\alpha^4,$$

$$c_3 = (7+1.5\cos\theta_2-\cos\theta_1)\alpha^2-(6+2.5\cos\theta_2-\cos\theta_1)\alpha^4,$$

where $\theta_1 = k_x h$, $\theta_2 = k_z h$, k_x and k_z are the wave-numbers in the x- and z-axis directions, respectively.

To keep the numerical calculation stable, it is necessary for the eigenvalues of the matrix *B* to satisfy the inequality $|\lambda(B)| \le 1$. From this inequality we obtain numerically the stability condition as follows

$$\alpha \le \alpha_{\max} \approx 0.527, \qquad \text{(B7)}$$

or

$$\Delta t \le \alpha_{\max}\frac{h}{c_0} \approx 0.527\frac{h}{c_0}.$$

Appendix C: Derivation of the dispersion relation

To minimize the dispersion error, in this appendix we derive the dispersion relation of the ONADM. For this, we consider the harmonic solution of equation (3) and substitute the solution

$$U_j^n = \begin{pmatrix} u_0 \\ v_0 \end{pmatrix} \exp\left[i(\omega_{num} n\Delta t + kjh)\right], \tag{C1}$$

into equations (3) and (A4) to (A7) to obtain the following dispersion equation

$$4(\cos\gamma - 1)^2 + 2(a+b)(\cos\gamma - 1) + ab - d\sin^2\theta = 0, \tag{C2}$$

where

$$\gamma = \omega_{num}\Delta t, \quad \theta = kh,$$

$$a = \alpha^2(1-\cos\theta)(4-2\alpha^2),$$

$$b = \alpha^2[3(4+\cos\theta) - 5(2+\cos\theta)\alpha^2],$$

$$d = 15\alpha^4(1-\alpha^2)^2.$$

Using the dispersion relation (C2), we obtain the ratio of the numerical velocity to the phase velocity c_0 as follows

$$R_{ONADM} = \frac{c_{num}}{c_0} = \frac{\gamma}{\alpha\theta}, \tag{C3}$$

where γ satisfies the dispersion equation (C2).

For comparison, in this section we also present the dispersion relations of Dablain's high-order compact schemes (Dablain, 1986). On the base of the Lax-Wendroff scheme, Dablain (1986) developed the high order compact methods with different accuracies as follows

$$\left(\frac{\partial^2 u}{\partial x^2}\right)_j^n = \frac{1}{\Delta x^2}\left[w_0 u_j^n + \sum_{i=1}^{M} w_i (u_{j+i}^n + u_{j-i}^n)\right], \tag{C4}$$

where *M*=2, 3, 4, and 5 denote the methods with accuracy of O(4,4), O(4,6), O(4,8), and O(4,10), respectively. These coefficients in equation (C4) are presented in Table C1.

Similarly, we can obtain the ratio of the numerical velocity to the phase velocity for the high order compact schemes with different accuracies as follows

$$R_{L-W} = \frac{c_{num}}{c_0} = \frac{\arccos(1+e/2)}{\alpha\theta}, \tag{C5}$$

where

$$e = \alpha^2 b + \frac{1}{6}\alpha^4 \left[-b + w_0 \cos\theta + \sum_{i=1}^{M} w_i [\cos(i+1)\theta + \cos(i-1)\theta] \right], \qquad \text{(C6)}$$

$$b = w_0 + 2\sum_{i=1}^{M} w_i \cos(i\theta). \qquad \text{(C7)}$$

Table C1. The coefficients of the L-W schemes with different accuracies (Dablain, 1986).

Methods	w_0	w_1	w_2	w_3	w_4	w_5
O(4,4)	-5/2	4/3	-1/12			
O(4,6)	-49/18	3/2	-3/20	1/90		
O(4,8)	-205/72	8/5	-1/5	8/315	-1/560	
O(4,10)	-2.927222	1.666667	-0.238095	0.039683	-0.004960	0.000317

Appendix D: Derivation of Theoretical Errors

1-D case

We rewrite equation (1) as follows

$$(D_{2t} - D_{2x})u = 0, \qquad \text{(D1)}$$

where $D_{2t} = \partial^2 / \partial t^2$ and $D_{2x} = c_0^2 \partial^2 / \partial x^2$ are the exact derivative operators with respect to time and space.

We can define the following ONADM temporal operator, derived from equation (3) and used equations (1) and (A4)

$$L_{2t} u_j^n = \frac{1}{\Delta t^2}\left[\delta_t^2 u_j^n - \frac{(c_0 \Delta t)^4}{12} \partial_{4x} u_j^n \right], \qquad \text{(D2)}$$

and the ONADM spatial operator

$$L_{2x} u_j^n = \frac{2}{\Delta x^2}\delta_x^2 u_j^n - \frac{1}{2\Delta x}\left(E_x^1 - E_x^{-1}\right)\partial_x u_j^n. \qquad \text{(D3)}$$

Then the first equation of the vector equation (3) can be written as follows

$$(L_{2t} - c_0^2 L_{2x})u_j^n = 0. \qquad \text{(D4)}$$

The operator error of the ONADM is computed by a Taylor series expansion. Omitting details, we obtain the following errors of temporal and spatial operators

$$(D_{2t} - L_{2t})u_j^n = -\frac{\Delta t^4}{360}\partial_{6t} u_j^n + O(\Delta t^6), \qquad \text{(D5)}$$

$$(D_{2x} - c_0^2 L_{2x})u_j^n = \frac{c_0^2 \Delta x^4}{360}\partial_{6x} u_j^n + O(\Delta x^6). \qquad \text{(D6)}$$

Using equation (1) and combining the above results, we obtain the theoretical error E_1 of the ONDAM operator

$$E_1 = [(D_{2t} - L_{2t}) - (D_{2x} - c_0^2 L_{2x})]u_j^n$$

$$= -c_0^2 \frac{(\alpha^4 + 1)\Delta x^4}{360} \partial_{6x} u_j^n + O(\Delta x^6 + \Delta t^6). \quad \text{(D7)}$$

From the ONADM algorithm we have known that we must solve the gradient of the displacement u at each time step. To keep the ONADM calculation stable, we should also give the stable condition of computing the gradient of the displacement.

Obviously, the gradient of the displacement u for the homogeneous case satisfies the following equation

$$\frac{\partial^2}{\partial t^2}\left(\frac{\partial u}{\partial x}\right) = c_0^2 \frac{\partial^3 u}{\partial x^3}. \quad \text{(D8)}$$

When we use the ONADM to solve equation (D8) to obtain the gradient of the displacement, we similarly have the following theoretical error E_2 of the ONDAM operator

$$E_2 = [(D_{2t} - L_{2t}) - (D_{2x} - c_0^2 L_{2x})]\partial_x u_j^n$$

$$= -c_0^2 \frac{(7\alpha^4 + 3)\Delta x^4}{2520} \partial_{7x} u_j^n + O(\Delta x^6 + \Delta t^6). \quad \text{(D9)}$$

2-D case

For the 2-D case, equation (2) and the first equation of the vector equation (4) can be rewritten as follows

$$(D_{2t} - D_{2x} - D_{2z})u = 0, \quad \text{(D10)}$$

and

$$[L_{2t} - c_0^2 (L_{2x} + L_{2z})]u_{i,j}^n = 0, \quad \text{(D11)}$$

where $D_{2z} = c_0^2 \partial^2 / \partial z^2$ is the exact derivative operator with respect to the space z, and the ONADM operators, derived from equations (4), (A8), and (A9), are defined as follows

$$L_{2t} u_{i,j}^n = \frac{1}{\Delta t^2}\left[\delta_t^2 u_{i,j}^n - \frac{(c_0 \Delta t)^4}{12}\left(\partial_{4x} + 2\partial_{2x2z} + \partial_{4z}\right)u_{i,j}^n\right], \quad \text{(D12)}$$

$$L_{2x} u_{i,j}^n = \frac{2}{\Delta x^2}\delta_x^2 u_{i,j}^n - \frac{1}{2\Delta x}(E_x^1 - E_x^{-1})\partial_x u_{i,j}^n, \text{ and} \quad \text{(D13)}$$

$$L_{2z} u_{i,j}^n = \frac{2}{\Delta z^2}\delta_z^2 u_{i,j}^n - \frac{1}{2\Delta z}(E_z^1 - E_z^{-1})\partial_z u_{i,j}^n. \quad \text{(D14)}$$

Considering the case of $\Delta x = \Delta z = h$ and omitting details, we obtain the following theoretical error E_1 of the ONDAM operator via the Taylor series expansion

$$E_1 = [(D_{2t} - L_{2t}) - (D_{2x} - c_0^2 L_{2x}) - (D_{2z} - c_0^2 L_{2z})]u_{i,j}^n$$

$$= -\frac{\Delta t^4}{360}\partial_{6t} u_{i,j}^n - c_0^2 \frac{\Delta x^4}{360}(\partial_{6x} + \partial_{6z}) u_{i,j}^n + O(\Delta t^6 + h^6). \quad \text{(D15)}$$

From equation (2) the gradient of the displacement *u* yields the following equations

$$\frac{\partial^2}{\partial t^2}\left(\frac{\partial u}{\partial x}\right) = c_0^2\left(\frac{\partial^3 u}{\partial x^3} + \frac{\partial^3 u}{\partial x \partial z^2}\right), \text{ and} \quad \text{(D16)}$$

$$\frac{\partial^2}{\partial t^2}\left(\frac{\partial u}{\partial z}\right) = c_0^2\left(\frac{\partial^3 u}{\partial x^2 \partial z} + \frac{\partial^3 u}{\partial z^3}\right). \quad \text{(D17)}$$

Using the ONADM to solve equation (D16) to obtain the first derivative of the displacement u with respect to *x*, we have the following theoretical error of the ONADM

$$E_2 = [(D_{2t} - L_{2t}) - (D_{2x} - c_0^2 L_{2x}) - (D_{2z} - c_0^2 L_{2z})]\partial_x u_{i,j}^n$$

$$= -\frac{c_0^2 h^4}{720}\left(\frac{6}{7}\partial_{7x} + 10\partial_{3x4z} + 6\partial_{2x5z} + 2\partial_{x6z}\right)u_{i,j}^n - \frac{\Delta t^4}{360}\partial_{6tx} u_{i,j}^n + O(\Delta t^6 + h^6)$$

$$= O(\Delta t^4 + h^4). \quad \text{(D18)}$$

Similarly, for solving equation (D17) by using the ONADM we have

$$E_3 = [(D_{2t} - L_{2t}) - (D_{2x} - c_0^2 L_{2x}) - (D_{2z} - c_0^2 L_{2z})]\partial_z u_{i,j}^n = O(\Delta t^4 + h^4), \quad \text{(D19)}$$

Acknowledgments

This work was supported by the MCME of China and the MITACS project ``New interior point methods and software for convex conic linear optimization with applications to solving VLSI circuit layout problems". The research of the second author was partially supported by the grant #RPG 249635-02 of the National Sciences and Engineering Research Council of Canada (NSERC), a PREA award from Ontario, and the above-mentioned MITACS project.

References

Blanch, J.O. & Robertsson, J.O.A., 1997. A modified Lax-Wendroff correction for wave propagation in media described by Zener elements, *Geophys. J. Int*., **131**, 381-386.

Dablain, M.A., 1986. The application of high-order differencing to the scalar wave equation, *Geophysics*, **51**, 54-66.

Fei, T. & Larner, K., 1995. Elimination of numerical dispersion in finite-difference modeling and migration by flux-corrected transport, *Geophysics*, **60**, 1830-1842.

Fornberg, B., 1987. The pseudospectral method: comparisons with finite difference for

the elastic wave equation, *Geophysics,* **52**, 483-501.

Geller, R.J. & Takeuchi, N. 1998. Optimally accurate second-order time-domain finite difference scheme for the elastic equation of motion: one-dimensional case, *Geophys. J. Int.*, **135**, 48-62.

Higdon, R.L., 1991. Absorbing boundary conditions for elastic waves, *Geophysics,* **56**, 231-241.

Igel, H., Mora, P. & Riollet, B., 1995. Anisotropic wave propagation through finite-difference grids, *Geophysics* **60**, 1203-1216.

Kelly, K., Ward, R., Treitel, S. & Alford, R., 1976. Synthetic seismograms: a finite-difference approach, *Geophysics* **41**, 2-27.

Konddoh, Y., Hosaka, Y. & Ishii, K., 1994. Kernel optimum nearly analytical discretization algorithm applied to parabolic and hyperbolic equations, *Computers Math. Appl.*, **27**, 59-90.

Kosloff, D. & Baysal, E., 1982. Forward modeling by a Fourier method, *Geophysics*, **47**, 1402-1412.

Mizutani, H., Geller, R.J. & Takeuchi, N., 2000. Comparison of accuracy and efficiency of time-domain schemes for calculating synthetic seismograms, *Phys. Earth Planet. Int.*, **119**, 75-97.

Richtmyer, R.D. & Morton, K.W., 1967. *Difference methods for initial value problems*, Interscience, New York.

Sei, A. & Symes, W., 1994. Dispersion analysis of numerical wave propagation and it computational consequences, *Journal of Scientific Computing*, **10**, 1-27.

Takeuchi, N. & Geller, R.J., 2000. Optimally accurate second order time-domain finite difference scheme for computing synthetic seismograms in 2-D and 3-D media, *Phys. Earth Planet. Int.*, **119**, 99-131.

Wang, S.Q., Yang, D.H. & Yang, K.D., 2002. Compact finite difference scheme for elastic equations, *J. Tsinghua Univ. (Sci. & Tech.)*, **42**, 1128-1131. (in Chinese)

Yang, D.H., Liu, E., Zhang, Z.J. and Teng, J., 2002. Finite-difference modelling in two-dimensional anisotropic media using a flux-corrected transport technique, *Geophys. J. Int*., **148**, 320-328.

Yang, D.H., Lu, M., Wu, R.S. & Peng, J.M., 2004. An Optimal Nearly-Analytic Discrete Method for 2D Acoustic and Elastic Wave Equations, *Bull. Seism. Soc. Am.*, **94**. (in press)

Yang, D.H., Teng, J.W., Zhang, Z.J. & Liu, E., 2003a. A nearly-analytic discrete method for acoustic and elastic wave equations in anisotropic media, *Bull. Seism. Soc. Am.*, **93**, 882-890.

Yang, D.H., Wang, S.Q., Zhang, Z.J. & Teng, J.W., 2003b. n-times absorbing boundary conditions for compact finite difference modeling of acoustic and elastic wave propagation in the 2-D TI Medium, *Bull. Seism. Soc. Am.*, **93**, 2389-2401.

Zhang, Z.J., Wang, G.J. & Harris, J.M., 1999. Multi-component wave-field simulation in viscous extensively dilatancy anisotropic media, *Phys. Earth Planet. Inter.*, **114** 25-38.